JOURNAL OF GEOPHYSICAL RESEARCH, VOL. 101, NO. A5, PAGES 11,039–11,053, MAY 1, 1996

# Electron and ion temperature gradients and suprathermal tail strengths at Parker's solar wind sonic critical point

J. D. Scudder

Department of Physics and Astronomy, University of Iowa, Iowa City

**Abstract.** New constraints are placed on the electron and ion temperature gradients at Parker's sonic point, demonstrated here as the location for an ion where the force of gravity and the electric field parallel to the magnetic field are balanced. The equal-temperature, one-fluid versions of these results precisely recover Parker's necessary and sufficient conditions for the supersonic expansion. The two species constraints are largely within the Parker envelope. For all possible critical points, the electron partial pressure must exceed 0.2437 of the plasma pressure at this point. The location of the critical point relative to the isothermal critical point is determined by the partial pressure average of the electron and ion logarithmic derivatives of temperature at the critical point. The bulk acceleration at the critical point is controlled by (1) the ion (as distinct from the electron) temperature gradient at this point and (2) the ratio of the ion to electron pressure at the critical point. The sonic point is a velocity space deLaval nozzle rather than a traditional configuration space nozzle. Critical points are most frequently accompanied by positive radial ion and electron temperature gradients. The electron and ion temperature gradients required for a critical point are coupled and not arbitrary. Parker's one-fluid discussion requires, by this analysis, both electron and ion temperature gradients to have positive radial exponents $\beta = 3/4$ near the critical point and a local effective gas polytrope behavior of $\gamma = 10/13 < 1$. For equal electron and ion temperatures, all possible critical points require positive ion temperature gradients at the critical point. Nonthermal electron and ion distributions are demonstrated to be generally required near the sonic critical point of a spherically symmetric solar wind. Effective polytrope exponents near the critical point range from $\gamma_i(r_*) < 1$ and $1.5 > \gamma_e(r_*) > 1/3$. The allowed critical points with $\gamma < 1$ are used to infer a range of nonthermal $\kappa$ distributions that permit this unusual $\gamma < 1$ behavior; ion nonthermal suprathermal tail indices ranging between $2 < \kappa_i < 5$ are required, reflective of decidedly nonthermal distributions at the critical point and consistent with previous inferences of their size [*Scudder*, 1992b]. Even when unequal electron and ion temperatures are considered, the vast preponderance of the critical points delineated also is found with $1/3 < \gamma_e < 1$, with the attendant range of electron nonthermal indices, $\kappa_e$, ranging from 2 to the Maxwellian limit of $\infty$. Critical points with maximal acceleration invariably occur for a positive electron temperature power law exponent of $\beta_e \simeq 1.12$ that corresponds to $\kappa_e \simeq 3.3$, whether or not the ions and electrons have a common temperature at the critical point.

## 1. Introduction

From his announcement of the hydrodynamic model of the coronal expansion, *Parker* [1964b] responded to numerous criticisms, especially from the exospheric community [*Chamberlain*, 1960, 1961, 1965]. *Parker*'s [1958] fluid picture predicted a transition near the coronal base to a supersonic "solar wind" flow, while the Chamberlain approach yielded the "solar breeze" solutions that were everywhere subsonic. Chamberlain held the idea (1) that the transition to collisionless behavior would make the coronal extension a form of evaporation that could be closely modeled with the tools of neutral exospheric theory; and (2) that such a model would asymptotically merge adiabatically with the surrounding medium of the star. The wind-breeze controversy was abruptly terminated by the observation of continuous supersonic flow by the interplanetary Mariner 2 spacecraft in 1962.

While the supersonic measurements repeatedly confirmed the wind picture, the theoretical premise of the exospheric approach and the soft theoretical arguments (in terms of Knudsen number) for a fluid's truncated description of the plasma in the vicinity of Parker's critical point were not redressed until *Jensen* [1963], *Brandt and Cassinelli* [1966], *Lemaire and Scherer* [1970], *Jockers* [1970], *Hollweg* [1970, 1971], and *Lemaire and Scherer* [1971] gave partial theoretical demonstrations that the supersonic solar wind solution could be obtained by exospheric methods. In their simplest form, Parker's arguments and those of the exosphericists employ conservation laws to determine how the wind accelerates. Because of this common thread and because of the common conservation law premise of both types of descriptions, there should be a feature to the exospheric solutions that corresponds to the sonic critical point elucidated by Parker.

This paper develops the idea that the formation of the su-



Paper number 96JA00188.
0148-0227/96/96JA-00188$09.00

personic transition in the exospheric framework is related to the form of the ion's electrical plus gravitational equivalent potential, $\Psi_+$, which in turn, is sensitive to the electron pressure profile in its vicinity.

Using energy dependent exobases, Brandt and Cassinelli reported exospheric solutions that were supersonic; however, they made their calculations in the presence of the electric field assumed by *Pannekoek* [1924] and *Rosseland* [1922] (PR), which is only appropriate for a static atmosphere. This PR field is inconsistent with the presence of quasi-neutral bulk acceleration, and it is also shown below to be incompatible with the formation of a critical point in a spherically symmetric geometry. Unlike his predecessors, Jockers realized that the electric field required for charge neutrality in a flowing plasma was substantially different from the PR field from static ion exospheres. Jockers asserted that the maximum of $\Psi_+$ was inside of, but nearly at, the gas dynamic sonic point, but he did not elaborate. Jockers also refers to a "critical" radius $r_c$ and the location of the maximum of the ion's equivalent potential $r_m$, with $r_c < r_m$. Jockers radial distance $r_c$ is critical, that is pivotal, to the solution of his transcendental equations and should not be confused with the specialized term "critical point" of a differential equation that figures so prominently in Parker's solution for the wind. Jockers did not seek to delineate the implications of this fact, nor analytically retrieve Parker's sonic point existence results. One group of his solutions for ions were parametric in assumed electron temperature profiles; in all but one solution the electrons were treated as a fluid: isothermal out to some radius and then falling as a shallow power, $\beta_e$, of radius between ($-\frac{1}{3}$ and $-\frac{1}{2}$). *Hollweg* [1970] considered exospheric ions and fluid electrons outside a radius which, in retrospect, is outside the critical point. Lemaire and Scherer considered exospheric solutions only above a peak in the equivalent potential without identifying it as the critical point. *Eviatar and Schulz* [1970] and *Schulz and Eviatar* [1972] considered the evolution of anisotropic convecting Maxwellians in monotonically decreasing potentials.

Parker's existence arguments for supersonic transitions did not presume whether or not there was a local or distributed energy addition to the corona in the vicinity of the critical point. By parameterizing the temperature profile in terms of its logarithmic derivative $\beta$ at the critical point, his analysis focuses on the conservation of matter and momentum and the range of $\beta$ that permits a supersonic transition. *Parker* [1963] established the conditions for a critical point in his Bernoulli equation: if, and only if, the radial power law exponent $\beta$ of the one-fluid temperature near the critical point was in the range

$$-1 < \beta < 2 \tag{1}$$

(Parker 1: fluid critical point condition). The $\beta > 0$ solutions have often been construed to allow distributed heat addition near the critical point. Since Parker's analysis does not use an energy equation, neither the maintenance of the temperature nor its gradient at the critical point is determined; only a range of gradients necessary for the supersonic expansion was established. If there had been an actual energy equation model, there would not be a range of allowable radial gradients at the critical point once the asymptotic boundary conditions were specified.

The analysis presented in this paper will also parameterize moment temperature profiles near the critical point as power laws, but now at the two-fluid level to permit discussion of the formation of a "critical point" in the exospheric description of the wind. The exospheric solutions must satisfy the same conservation laws of matter and momentum as the fluid description. The language of these constraints is the moments over the velocity distributions. These quantities can be evaluated either from the fluid theory or the exospheric theory. These theories have a different view of how the energy is transported and the distribution functions reshaped. These theories have solutions that require different levels of detail about the forces experienced by individual particles versus the average force felt by the fluid as a whole.

Establishing the plasma physics in the vicinity of the critical point, rather than the gas dynamics of it, is the focus of this paper. This paper derives *Parker*'s [1964a, p. 76] inequality (1) as a restatement that the critical point must be where the ion equivalent potential has a local maximum. The generalized Ohm's law is used to define the equivalent ion potential in terms of the electron moment parameters. The range of radial gradients of electron and ion temperatures at the critical points implies constraints on the nonthermal distributions if they, by themselves, explain the radial variations. The suprathermal behavior determined in this way has many of the properties required by earlier independent arguments [*Scudder*, 1992a, b, 1994] that pertain to a new explanation for why the corona is hotter than the chromosphere.

A companion paper [*Scudder*, 1996] uses the location and single-particle force physics of this critical point location to illustrate the very large size of the parallel electric field that is found at the critical point and discusses its implications for post Chapman-Enskog transport in its vicinity.

## 2. The Fluid Critical Points of Parker

The Parker critical point at $r_*$ in a spherically symmetric expansion is determined implicitly by the locations where the following Bernoulli form of the one-fluid momentum equation is of the indeterminate 0/0 form:

$$\frac{1}{U}\frac{dU}{dr} = \frac{(2V_t^2/r) - (dV_t^2/dr) - (GM_S/r^2)}{(U^2 - V_t^2)}, \tag{2}$$

where $V_t^2 = 2k\langle T\rangle/(M + m)$ and $\langle T\rangle$ is the one-fluid temperature $\langle T\rangle \equiv (T_e + T_p)/2$. Equivalently, $V_t^2$ is, in fact, the square of the isothermal ion sound speed [e.g., *Krall and Trivelpiece*, 1973]. At $r_*$, only a portion (cf. Appendix A) of the one-fluid pressure gradient force equals the gravitational force on the composite fluid.

Paralleling Parker's ansatz, a power law variation near the critical point, $r_*$, is assumed for the temperature of the form

$$\langle T\rangle = T_*(r_*)\left(\frac{r}{r_*}\right)^{\beta}. \tag{3}$$

The power law exponent $\beta$ is the logarithmic derivative of the temperature at the critical point if distances are measured in units of the critical radius. A critical point is possible when (from the denominator of (2)) the bulk speed equals the isothermal ion sound speed determined by the local temperature $T_*$,

$$U_*(r_*) = V_t(r_*), \tag{4a}$$

at the point $r_*$ (from the numerator of (2)) defined by the relation

$$r_* = \frac{GM_S(M + m)}{2kT_*(2 - \beta)}. \tag{4b}$$

For future reference, the isothermal critical point radius determined by $\beta = 0$ is defined as

$$r_{*,\mathrm{iso}} = \frac{GM_S(M + m)}{4kT_*}. \tag{4c}$$

The original critical point form of the Bernoulli equation in (2) may be recast in the succinct form

$$\frac{1}{v}\frac{dv}{d\chi} = \frac{(2-\beta)(\chi^{\beta-1} - \chi^{-2})}{v^2 - \chi^{\beta}}, \tag{5a}$$

after rescaling the flow speed in units of its value $V_t(r_*)$ at the critical point

$$v \equiv \frac{U}{U_*}, \tag{5b}$$

and distance in units of $r_*$, the still unknown "critical point" location

$$\chi \equiv \frac{r}{r_*}. \tag{5c}$$

In order that the spatial derivative of speed from (5a) be nonzero and finite at $r_*$, the l'Hospital limit of (5a) must exist at the critical point: $\chi = 1$, where $v = 1$ also. This condition implies that the acceleration at $\chi = 1$ where this might be possible must satisfy the quadratic equation

$$2\left(\frac{d\ln v}{d\chi}\right)^2\Big|_1 - \beta\left(\frac{d\ln v}{d\chi}\right)\Big|_1 + (\beta-2)(\beta+1) = 0. \tag{5d}$$

The roots of this equation may be written as

$$\left(\frac{dv}{d\chi}\right)\Big|_1^{\pm} = \frac{\beta \pm \sqrt{\beta^2 - 8(\beta-2)(\beta+1)}}{4}. \tag{6}$$

The existence of a saddle point (X-type) requires that the above roots for $(dv/d\chi)|_1$ be real and of opposite sign [cf. *Simmons*, 1972]; these two conditions are simultaneously met by the inequality

$$(\beta-2)(\beta+1) < 0, \tag{7a}$$

since (7a) guarantees that the absolute value of the discriminant term in (6) can always reverse the sign of the acceleration under the $\pm$ options. Condition (7a) is equivalent to the requirement

$$-1 < \beta < 2, \tag{7b}$$

retrieving *Parker*'s [1964a] original condition (cf. (1)) on the temperature profile to guarantee a critical point.

## 3. The Exospheric Thesis About Critical Points

The purpose of the present paper is to demonstrate those properties of the exospheric solutions essential for a critical point to form. If properly implemented, the exospheric solution conserves both matter and momentum. Of course, the conservation law constraints are common to both fluid and exospheric descriptions. Although some authors have produced "supersonic" exospheric solutions that are said to support the uniqueness of the wind interpretation, the essential ingredients of the exospheric solutions which permit supersonic flow to be achieved have not been identified until now. Neither has the generality of Parker's critical point condition been retrieved in the exospheric context. Jockers demonstrated with a graphical analysis that a nonmonotonic potential different from that suggested by *Pannekoek* [1922] and *Rosseland* [1924] was required for his supersonic solution. This paper demonstrates analytically that the location $r_*$ of the critical point in the flow in the exospheric solution is that radial location where the equivalent ion potential for the parallel microscopic forces, $\Psi_+$, is positive, and a local maximum. For clarity, we separately denote this exospheric point by $r_{\Psi_+}$. Once this relationship is established, we use it to develop further constraints on the temperature gradients, the local polytrope indices, and suprathermal tails needed to form this nonmonotonic equivalent potential.

To motivate that this hypothesis is indeed likely, a brief heuristic discussion is in order.

First, it can be shown by the method of characteristics that under these conditions, the ion fluid speed (determined by moments) at such a point is always above, but of the same order as, the ion thermal and, hence, sound speed at this location in parallel with (4a) above.

Second, the equivalent potential $\Psi_+$ for ions reflects a competition between the extracting electric field and the attracting gravitational force. Clearly, the ions that surmount the local maximum in $\Psi_+$ continue to increase their bulk speed further, being accelerated as they fall back down the equivalent potential. Since the system is momentum dominated, and the electric field involved in this balance must be consistent with quasi-neutrality, the acceleration of the ions through this point guarantees that the plasma as a whole does so.

Thus the two basic ingredients of the saddle-type X-point of the fluid equations are properties of a collisionless solution in the presence of such a nonmonotonic ion effective potential.

Depending on the spatial profile of the electrical potential, $\Psi_+$ can be negative definite (as in the Pannekoek-Rosseland electric field) or monotonic or, while changing sign, can be simply nonmonotonic or possess multiple minimaxes. The role of the electric force is to enhance the electron binding to the star to enable quasi-neutral, but inhomogeneous profiles. Since the quasi-neutralizing electric force on electrons is alway aligned with the gravitational force, its equivalent potential $\Psi_-$ is always negative definite with respect to infinity. Since the total electron force must always be toward the Sun, its equivalent potential $\Psi_-$ must be monotone increasing. The competition between the electric and gravitational forces notationally "disappears" in the one-fluid description (except in the generalized Ohm's law); the physics of this competition with the electric force remains, however, in the divergence of the electron portion of the pressure tensor and is reflected in the velocity distribution functions of the constituents.

Consider the consequences of $\Psi_+$ having a single local maximum value, $\Psi_0(r_{\Psi_+})$, at some location $r_{\Psi_+}$ above the solar surface. No particles of the inner radial boundary distribution function with initial kinetic energy below $\Delta\Psi = |\Psi_0 - \Psi_+|$ can get past $r_{\Psi_+}$. If, as is suggested from Jockers' work, $\Psi_0 > 0$, the effective potential must then decrease beyond this point toward the zero boundary value at infinity. Accordingly, ions that pass $r_{\Psi_+}$ will not return. Since no particles are assumed incident on the solar cavity at large distances ($P_\infty \to 0$), the distribution function at $r_{\Psi_+}$ is just that portion of the inner boundary distribution function with initial kinetic energy above $|\Delta\Psi|$, downshifted in energy enroute by $|\Delta\Psi|$ and moving outward. Such a local maximum places a filter in velocity space

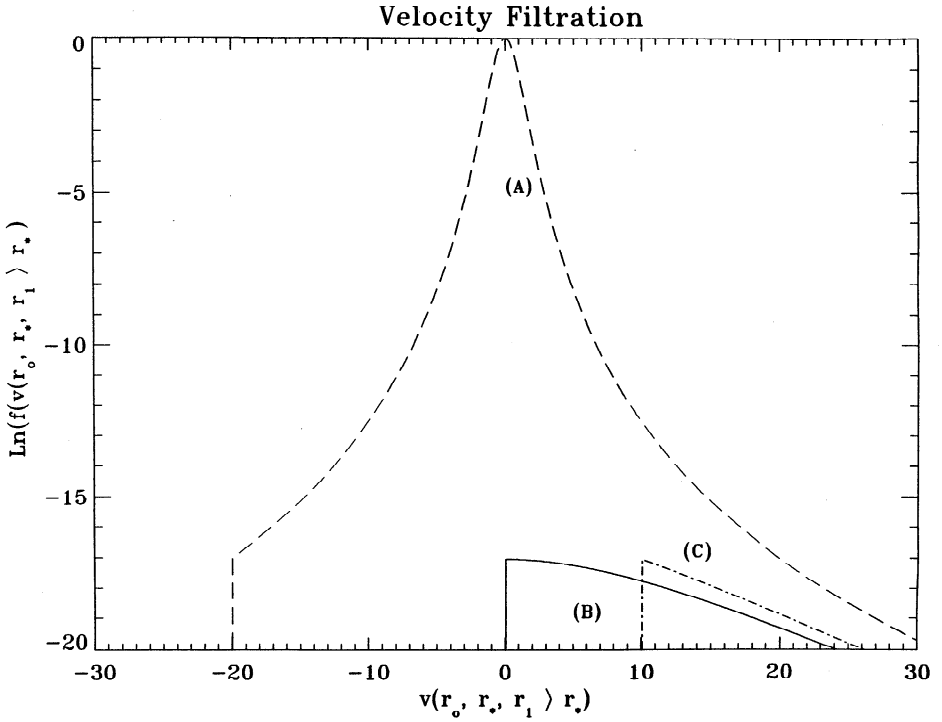


**Figure 1.** Details of velocity space below, at, and above the critical point.

(total kinetic energy) that determines the asymptotic escaping number flux. This potential barrier in phase space prevents low-speed particles from escaping the reservoir of the bound atmosphere. This is analogous to the geometric shape of the deLaval nozzle, which precludes gas molecules from ballistically participating in the exhaust if they are directed toward the confining container boundary where they are reflected in configuration space. (This connection is explored more fully in Appendix B.)

The ion distribution function at the radial inner boundary, at $r_{\Psi_+}$, and at some point well beyond $r_{\Psi_+}$ is illustrated in Figure 1. The crucial features of the distribution at $r_{\Psi_+}$ illustrated in Figure 1, curve B, are that its peak is at the local origin of velocity space, and that the entire distribution of populated orbits is moving away from the Sun at $r_{\Psi_+}$. This type of distribution has the generic property that its bulk speed and its thermal spread about the mean bulk speed $U$ are very nearly the same. As an example, assume that $f$ at $r_{\Psi_+}$ was a velocity-filtered kappa distribution [*Scudder*, 1992a]:

$$f(v, r_{\Psi_+}) = \Theta(v_\parallel)\Theta\left(\frac{\beta(v_\phi^2 + v_\parallel^2)}{1-\beta} - v_\perp^2\right) \cdot \frac{A_\kappa}{\pi^{3/2}w_c^3}\frac{1}{[1 + (v^2 + v_\phi^2)/\kappa w_0^2]\kappa + 1}, \quad (8)$$

where $\Theta(x)$ is the Heaviside function, $\beta = B(r_{\Psi_+})/B(r_0)$, and the potential energy barrier to the local maximum from the lower boundary condition is

$$\tfrac{1}{2}Mv_\phi^2 = |\Psi_+(r_*) - \Psi(r_0)|.$$

The bulk speed variation at the maximum of $\Psi_+$ has been surveyed, as it depends on the potential difference and the magnetic intensity ratio between the transition region boundary at $r_0$ and the $r_{\Psi_+}$. The maximum and minimum variations of the ion sonic Mach number as a function of $\kappa$ assumed is illustrated in Figure 2. Extreme values of the ion sonic Mach number after scanning all combinations of $1 < v_\Phi^2/w_0 < 10^5$ and $10^{-5} < \beta < 1$ for a spectrum of $\kappa$ values are indicated by the solid traces in Figure 2. The entire solution space for all $\kappa$ exceeds unity, as is suggested by Figure 1. Thus the suggested location is consistent with the entire plasma passing through a sonic point at this location.

The precise size of the ion acoustic speed depends also on the electron temperature at $r_*$, not included in this thermal Mach number estimate. When the estimates of the critical points agree as required below, then the zero in the denominator of (2) will occur as the one-fluid conservation laws require with $U(r_*) = [k(T_{e,*} + T_{i,*})/(M + m)]^{1/2}$, that is, acoustic Mach number unity.

From the difference of the electron and ion momentum conservation equations, it is easy to show that the onset of outward bulk acceleration of the fluid necessitates a strengthening of the electric field to maintain quasi-neutrality, viz.,

$$\mathbf{E} = -\nabla\Phi_E = \frac{M-m}{2|e|}\nabla\Phi_G + \frac{M-m}{2|e|n}\nabla\cdot(n\mathbf{VV}) + \frac{\nabla\cdot(\mathbf{P}_i - \mathbf{P}_e)}{2|e|n} + \frac{\zeta_{\text{exchange}}}{|e|n}, \quad (9)$$

where $\zeta_{\text{exchange}}$ corresponds to the net frictional force on electrons from ions. The first term of (9) is that retained in the Pannekoek-Rosseland estimates of the electric field neglecting flow or pressure differences in the plasma. The equivalent potential energy $\Psi_+$ for ions is given by the expression

$$\Psi_+ = e\Phi_E - \frac{GM_SM}{r}, \quad (10)$$

where $\Phi_E$ is the electrical potential and is always positive in order to restrain the electron's mobility. Steady fluid expansion

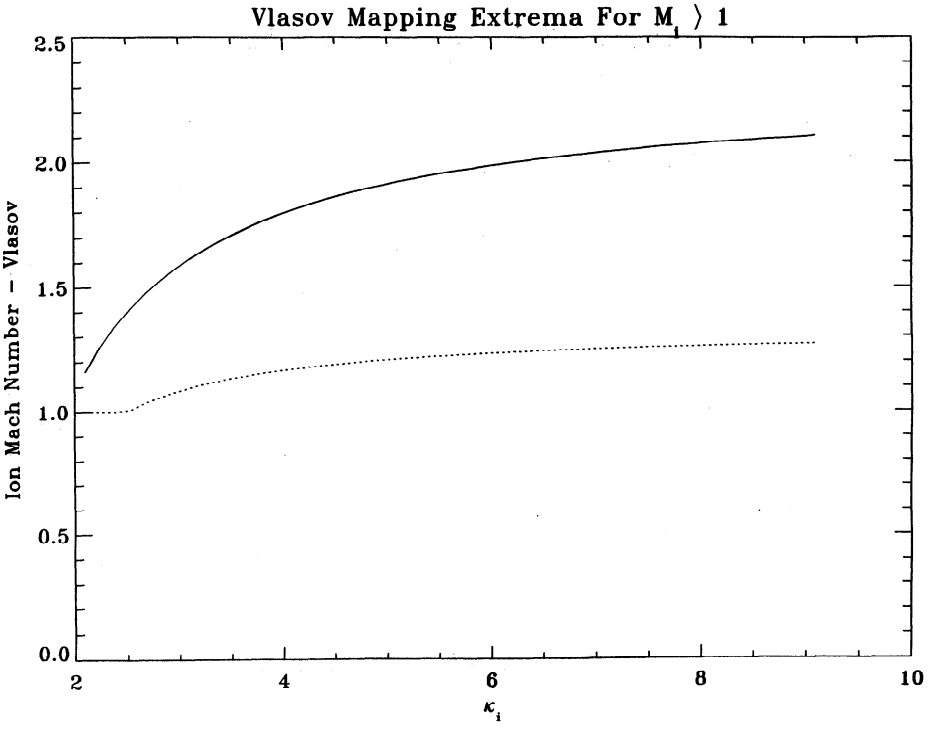


**Figure 2.** The range of ion Mach number $M_i$ as a function of $\kappa$ for a Vlasov mapped truncated kappa distribution. A wide range of possible changes in magnetic intensity and potential barrier height have been surveyed to infer this possible range of $M_i$.

can reverse the sign of the ion's equivalent potential by influencing $\Phi_E$ without reversing the sign of the electron's potential, $\Psi_- = -e\Phi_E - GM_S m/r < 0$. The electron potential must remain monotonic so that the force is toward the Sun. Since the zero of potential is at infinity, this possible reversal in the sign of the ion's equivalent potential must then lead to a minimax for $\Psi_+(r)$. The conjectured requirements for a critical point can be summarized as

$$e\Psi_+(r_{\Psi_+}) > 0 \tag{11a}$$

$$\left.\frac{d\Psi_+}{dr}\right|_{r_{\Psi_+}} = 0 \tag{11b}$$

$$\left.\frac{d^2\Psi_+}{dr^2}\right|_{r_{\Psi_+}} < 0 \tag{11c}$$

The electric field that regulates the quasi-neutrality of the plasma is the ambipolar electric field. Therefore the leading-order form of this electric field from the electron momentum equation is

$$\mathbf{E} = -\nabla\Phi_E \simeq -\frac{\nabla\cdot\mathbf{P}_e}{en_e} - \frac{GM_S m}{er^2}\hat{\mathbf{r}} + O\left(m, \frac{\partial}{\partial t}, \nu_{ei}\right). \tag{12}$$

Assuming that the electron pressure is isotropic and that the electron temperature and density are power laws in the vicinity of the local maximum at $r_{\Psi_+}$ of the form

$$T_e(r) = T_{e*}\left(\frac{r}{r_{\Psi_+}}\right)^{\beta_e} \tag{13a}$$

$$n_e(r) = N_{e*}\left(\frac{r}{r_{\Psi_+}}\right)^{\delta}, \tag{13b}$$

the electron pressure near the critical point varies as

$$P_e = P_{e*}\left(\frac{r}{r_{\Psi_+}}\right)^{\delta+\beta_e} \tag{14a}$$

$$= P_{e*}\left(\frac{n}{n_e(r_{\Psi_+})}\right)^{\gamma_e(r_{\Psi_+})}, \tag{14b}$$

where $\gamma_e(r_{\Psi_+}) = (\delta + \beta_e)/\delta$. Condition (11b), imposed at $r_{\Psi_+}$, is thus equivalent to the condition

$$(-\delta - \beta_e) = \frac{[GM_S(M+m)/r_{\Psi_+}]}{kT_{e*}} > 0, \tag{15a}$$

or that the radius of the local maximum of $\Psi_+$ should be at

$$r_{\Psi_+} = \frac{GM_S(M+m)}{kT_{e*}(-\delta-\beta_e)} \tag{15b}$$

For future differentiation, $d\Psi_+/d\chi$ can be written in terms of $r_{\Psi_+}$ of (15b) and the dimensionless length $\chi$ in the form

$$\frac{d\Psi_+}{d\chi} = kT_{e*}(-\delta-\beta_e)(\chi^{\beta_e-1} - \chi^{-2}). \tag{16}$$

Using (16), the local maximum condition (11c) becomes

$$\left.\frac{d^2\Psi_+}{d\chi^2}\right|_{\chi=1} = kT_{e*}(-\delta-\beta_e)(\beta_e+1) < 0. \tag{17a}$$

This condition (upon using (15a)) is equivalent to the relation

$$-1 < \beta_e < -\delta. \tag{17b}$$

The spherical form of the conservation of electrons in dimensionless variables near the critical point takes the form

$$v = \chi^{-2-\delta}. \tag{18}$$

Clearly, $v$ cannot be an increasing function of distance at the critical point and beyond unless

$$-\delta > 2 \tag{19}$$

(expansion condition). Conditions (19) and (17b) combine to say that whatever value $\delta$ is used for the solution, it must be such that

$$-1 < \beta_e < 2 < -\delta \tag{20}$$

(local maximum at $\Psi_+(r_{\Psi_+})$). The first nested set of inequalities in (20) for $\beta_e$ is precisely that summarized by Parker's one-fluid discussion for the one-fluid and the common-fluid temperature variation (cf. (7b)).

With the $\Psi_+$ discussion, it can be seen that Parker's constraints on the "common," but equal temperature profiles are actually selecting from all possible electron pressure variation profiles those with a suitably sized electric field to compete with gravity and make the nonmonotonic impediment to ions leaving the Sun.

However, the formulae for the critical point (3b) of the fluid and local maximum of $\Psi_+$ (15b), although of similar structure, are not precisely the same. From the conservation law (one-fluid) and exospheric viewpoint the critical point determined by (15b) from the electron and ion kinetic behavior is also determined for the fluid as a whole by (3b). In order that $r_* = r_{\Psi_+}$ under *Parker*'s [1964a] assumption that the electron and ion temperature profiles have the same radial power law variation in the vicinity of the critical point, we must have

$$\frac{GM_S(M+m)}{2kT_*(2-\beta_e)} = \frac{GM_S(M+m)}{kT_{e*}(-\delta-\beta_e)}, \tag{21a}$$

which implies that

$$-\delta - \beta_e = 2(2-\beta_e). \tag{21b}$$

With the assumed form of the density variation

$$\delta(r_{\Psi_+}) \equiv \left.\frac{d\ln n}{d\chi}\right|_{\chi=1}, \tag{22a}$$

the mass conservation condition condition at the critical point implies that

$$-\delta = 2 + \left.\frac{d\ln v}{d\chi}\right|_{\chi=1}. \tag{22b}$$

Using (22b) in (21b) yields the compatibility condition that the one-fluid critical point be at the maximum in $\Psi_+$:

$$\left.\frac{d\ln v}{d\chi}\right|_1 = 2 - \beta_i \equiv 2 - \beta_e > 0 \tag{23a}$$

(one fluid). Inserting this condition in (5d) determines the constraint on the value(s) of $\beta_e = \beta_i$ required, viz., as solutions to

$$(2-\beta_e)(4\beta_e - 3) = 0 \qquad \beta_e = \beta_i \tag{23b}$$

There is only one root to (23b) in the range allowed by (23a), namely, at $\beta^*_{e,i} = \frac{3}{4}$. Because $\delta$ at this location is also determined from (21b), the effective local electron/ion polytrope exponent can be inferred from the relationship

$$\gamma^*_{e,i}(r_*) = \frac{\delta + \beta^*_{e,i}}{\delta} = \frac{10}{13} \simeq 0.77 < 1 \tag{24}$$

(one fluid). Eschewing the interpretation of (24), that this implies local heat deposition in the vicinity of the critical point, an approximate value of the nonthermal index $\kappa$ that would be required for electrons and ions if they had the same profile in the vicinity of the critical point is given by the relation derived by *Scudder* [1992b],

$$\kappa_{e,i}(r_*) = \frac{3-\gamma^*}{2-2\gamma^*}, \tag{25a}$$

that takes on the value in the present circumstances of

$$\kappa_{e,i}(r_*) = \tfrac{29}{6} \simeq 4.8 \tag{25b}$$

(one-fluid behavior approximation).

It is exceedingly unlikely that the ions and electrons will have the same thermal gradients near the critical point: (1) it is well known that their effective potentials are different in this area; (2) even if both species had local power law behaviors, their sum is in general not a power law, though it is assumed to be in the Parker derivation; and (3) the high mobility of the electrons implies (as in the two-fluid models of *Sturrock and Hartle* [1966]) that their temperature profile is not proportional to that of the ions.

The physics of the nonmonotonic profile of $\Psi_+$ is that demanded by quasi-neutrality in an expanding medium (9), a topic that is only addressed in the Parker model by the use of a common continuity equation for electrons and ions. For example, a given ad hoc temperature profile or polytrope assignment need not be microscopically consistent with quasi-neutrality. Many of the mathematically possible profiles admitting subsupersonic transitions are not (according to (7b) and (20)) consistent with quasi-neutrality. Perhaps this may be seen more readily by recalling that the location of the critical point is that location where for the one-fluid picture and the quasi-neutrality picture to be consistent, a rather specific radial profile of the electron temperature is required so that the electrons can perform their role through $\Phi_E$ in making the nonmonotonic profile of $\Psi_+$, yet be consistent with the steady state one-fluid dynamics that is (only) superficially independent of the electric field. Furthermore, this radial profile requires that the one-fluid effective polytrope be less than unity, a result that would surely have dissuaded early borrowers of gas dynamical ($\gamma \geq 1$) descriptions for plasmas. A plasma can, however, support this type of behavior with appropriate nonthermal velocity distributions even without wave deposition [*Scudder*, 1992a]. The required size of the nonthermal index $\kappa$ in (25b) is well removed from the Maxwellian regime ($\kappa \to \infty$) and consistent with earlier requirements to explain the formation of the solar corona [*Scudder*, 1992b] and the observed mass flux of the solar wind [*Scudder*, 1994].

## 4. Two-Fluid Behavior at Critical Point: Common $T_*$

Assuming that the electrons and ions have the same temperature but different radial variations at the critical point yields a more realistic comparison of the implications of re-

quiring the location where $\Psi'_+ = 0$ to correspond to Parker's sonic critical point. This partition also illustrates the different role of the electron and ion temperature profiles in producing the supersonic transition. With common temperatures, the electrons and ions are both in the form of (potentially different) power laws

$$T_{e,i} = T_*\left(\frac{r}{r_*}\right)^{\beta_{e,i}}, \tag{26}$$

the two-fluid critical point generalization of (3b) takes the form

$$r_* = \frac{GM_S(M+m)}{kT_*[4-(\beta_e+\beta_i)]}. \tag{27}$$

This relationship checks with Parker's result (4b) in the common profile limit where $\beta_e \equiv \beta_i$.

From (27) it is clear that, for critical points to occur at finite positive radial distances,

$$\beta_i < 4 - \beta_e \tag{28}$$

must be enforced. The X-point behavior via l'Hospital's condition analogous to (5d) requires that the acceleration at the critical point satisfy

$$2\left(\frac{d\ln v}{d\chi}\right)^2\Bigg|_1 - \frac{\beta_i+\beta_e}{2}\frac{d\ln v}{d\chi}\Bigg|_1 + \left(\frac{\beta_i^2+\beta_e^2}{2} - \frac{\beta_i+\beta_e}{2} - 2\right) = 0. \tag{29}$$

Enforcing that the roots of (29) are real and of opposite signs implies that $\beta_{i,e}$ must be within the displaced circle of radius $3/2^{1/2}$ given by the equation

$$\frac{(\beta_i - \frac{1}{2})^2}{9/2} + \frac{(\beta_e - \frac{1}{2})^2}{9/2} < 1. \tag{30}$$

The condition of (30) implies that (28) is satisfied for physical roots at positive $r$ and that possible critical points occur over a restricted range of radial locations for a given temperature at the critical point $T_*$.

The exospheric local maximum point $r_{\Psi_+}$ (15b) can now be equated to the two-fluid conservation law picture of the critical point embodied in (27) to give the defining equation for the matched pairs of $\beta_{e,i}$ that are simultaneously in accord with an exospheric and a conservation law description, viz.,

$$\frac{GM_S(M+m)}{kT_*[4-(\beta_e+\beta_i)]} = \frac{GM_S(M+m)}{kT_*(-\delta-\beta_e)}. \tag{31a}$$

Using continuity (22b) to eliminate $\delta$ in (31a) implies that

$$\frac{d\ln v}{d\chi}\Bigg|_{\chi=1} = 2 - \beta_i > 0, \tag{31b}$$

which implies that

$$\beta_i < 2 \tag{31c}$$

is required for positive acceleration at the critical point. It is thus clarified that if $T_{e*} = T_{i*}$, the ion temperature gradient at the critical point determines the acceleration of the wind at the critical point and that the electron temperature gradient controls the existence of the nonmonotonic potential. In Parker's original discussion with $\beta_e \equiv \beta_i$, these separate roles in the dynamics and kinematics are degenerate.

Using (31c) in the quadratic formula of (29) yields the relation between $\beta_e$ and $\beta_i$ necessary to assure that the two-fluid descriptions via conservation law and the exospheric treatment's nonmonotonic potential $\Psi_+$ agree on the location of the critical point:

$$6\beta_i^2 + \beta_i(-19+\beta_e) + (12 - 3\beta_e + \beta_e^2) = 0. \tag{31d}$$

Given the solutions of (31d) and the implied value of $\delta$ (via (22b)) that goes with each pair, the effective $\gamma$ for each species in the vicinity of the critical point can be determined by (24). Noting when $\gamma < 1$ that such behavior can be mimicked by velocity filtration [*Scudder*, 1992a], a lower limit on such acceptable $\gamma$ is associated with velocity distributions having a finite pressure ($\kappa > 2$), which in turn, implies that a further constraint should be imposed of the form

$$\gamma_{e,i} > \tfrac{1}{3}. \tag{31e}$$

Condition (31e) together with (25a) and (24) yields the two further inequalities

$$\beta_i < \tfrac{8}{5} \qquad (\gamma_i > \tfrac{1}{3}) \tag{31f}$$

(two fluid) and

$$\beta_i < 4 - \tfrac{3}{2}\beta_e \qquad \gamma_e > \tfrac{1}{3} \tag{31g}$$

(two fluid).

The results for $\beta_i$ restricted by the inequalities of the circle of (30), the line of (31b), the equality given by the ellipse of (31d), and the inequalities of (31e–31g) are illustrated in Figure 3. The heavy curve between the terminating solid dots is the two-fluid solution set for $(\beta_e, \beta_i)$ with common $T_*$; the third dot between the extremities is the previously determined location with $\beta_e = \beta_i = \frac{3}{4}$, where Parker's condition and the minimax in the ion equivalent potential are in agreement at the one-fluid level of description. (The effect of not incorporating the conditions on $\gamma_{e,i}$ of (31e) would permit the acceptable solutions to proceed along the rotated ellipse up to $\beta_i = 2^-$ at the leftmost extremity and extend to the right toward the first intersection of the ellipse and the circle at approximately $\beta_e \simeq 2.5$.)

Of special interest is the fact that, with or without the conditions (31e–31g), the radial power law for ion temperature in the vicinity of the critical point is required to be positive, reflective of an ion temperature increasing with increasing radius at $r_*$. As this is a location where the density is decreasing, this type of behavior cannot be achieved with a traditional polytrope with $\gamma > 1$. Since all $\beta_i > 0$ for any $\beta_e$ allowed, $\beta_e$ has been used as the ordering parameter of the restricted set of solutions that meet the above inequalities and conditions. The smallest acceptable $\beta_e$ occurs with the $(\beta_e, \beta_i)$ pairs of $(-1.17, 1.60)$, and the largest with $(2.09, 0.859)$. Of interest is that the common isothermal $(\beta_e = \beta_i = 0)$ solution at common $T_*$ is also excluded. For comparison, the range of electron temperature variations determined or assumed by Jockers is also indicated. For the solutions where this radial variation was assumed, the electron temperature was constant out to $9R_S$ so that $\beta_e \simeq 0$ was the behavior of most of his solutions near the maximum in the potential. The one electron and ion exospheric solution attempted by Jockers had a slight negative

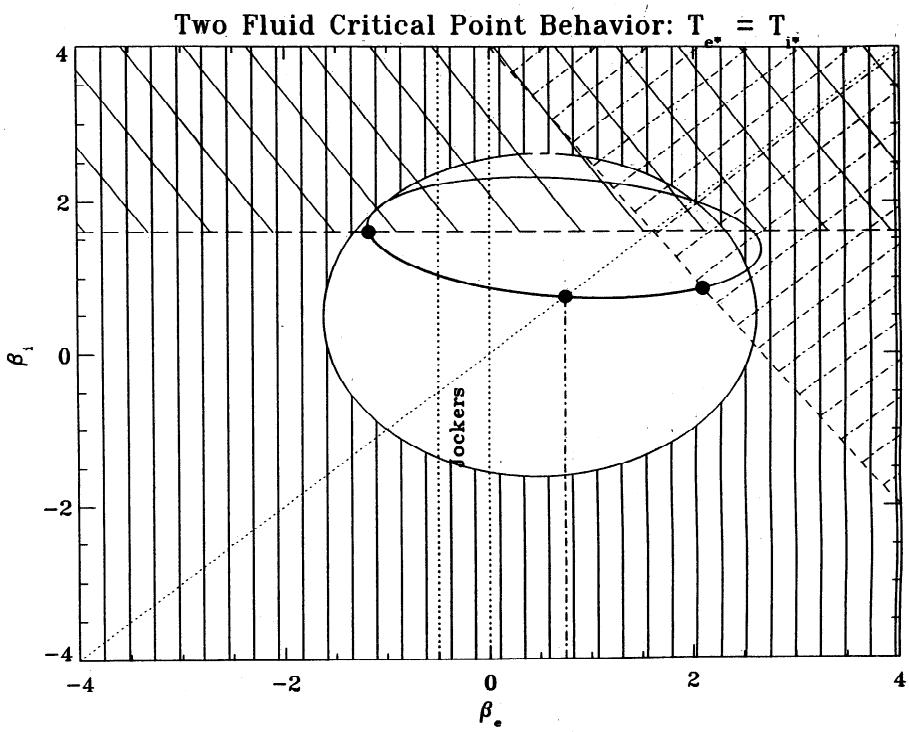


**Figure 3.** Two-fluid common temperature: solution space ($\beta_e$, $\beta_i$). Solution set indicated by the portion of rotated ellipse, inside the circle, indicated with heavy curve terminated with solid dots.

electron temperature gradient at the critical point of approximately the size indicated.

The acceptable ordered pairs ($\beta_e$, $\beta_i$) of Figure 3 determine the range of locations of the critical point $r_*$ possible from (27). These locations are indicated in Figure 4 in units of the isothermal critical point $r_{*,\mathrm{iso}}$ given by (4c). The acceptable locations range from 1 to 4 times that of the isothermal critical point. The isothermal critical points are found at $r_{*,\mathrm{iso}} = 5.7(10^6/T_*)R_S$, which makes the inferred location of the critical points of this discussion between

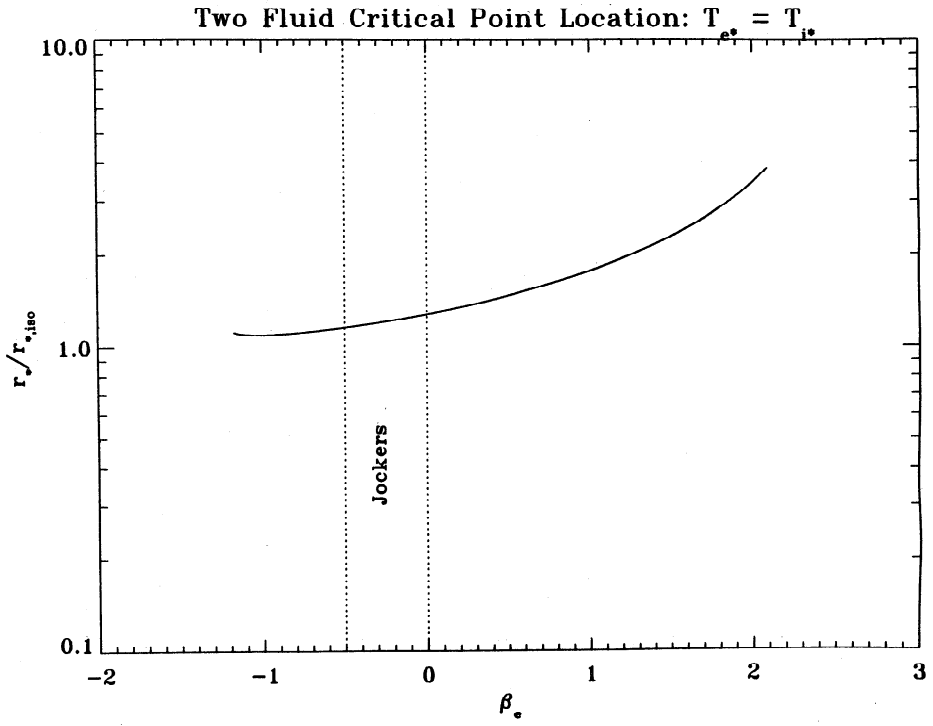


**Figure 4.** Two-fluid common temperature: critical point locations for solution set of Figure 3 in units of the isothermal critical point location given by (4b) and (4c).

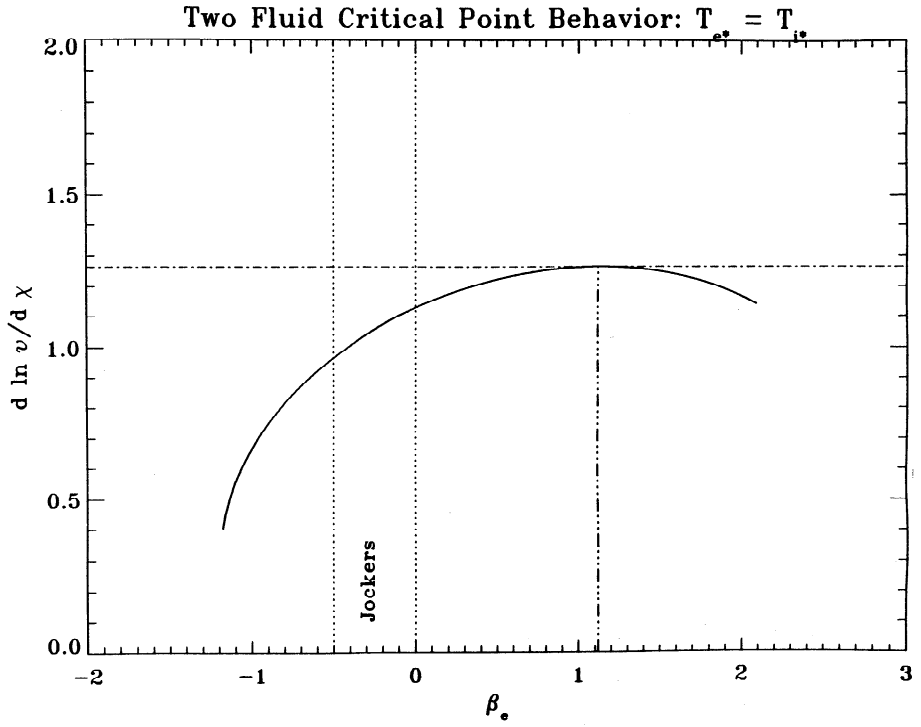


**Figure 5.** Two-fluid common temperature: accelerations at the critical point for solution set of Figure 3. Maximum acceleration for $\beta_e = 1.12$ corresponding to an electron $\gamma_e < 1$.

$$5.7\,\frac{10^6}{T_*}R_S < r_* < 23\,\frac{10^6}{T_*}R_S, \tag{32}$$

clearly in an acceptable range.

The acceleration at the critical point determined by the acceptable family of ion power law exponents via (31b) is illustrated in Figure 5. Of note is the inferred maximum acceleration at $\beta_e \simeq 1.12 > 0$. This corresponds to a local behavior in the electrons, if it were in the kappa family, of $\kappa_e(r_*) \simeq 3.3$, also consistent with previous indications of its size to explain the coronal temperature inversion [*Scudder*, 1992b, 1994]. The logarithmic derivative of the density $\delta(r_*)$ at the critical point is illustrated in Figure 6 and reflects the faster than inverse square density falloff required by the transonic wind solution to achieve the positive acceleration at the critical point.

The local polytrope behavior at the critical point is determined from the acceleration and the continuity equation by the relationship

$$\gamma_{\text{eff}\,e,i}(r_*) = 1 + \frac{\beta_{e,i}}{2 - [(d\ \ln\ v)/d\chi]} = \frac{\beta_{e,i} + \beta_i - 4}{\beta_i - 4}. \tag{33}$$

All the $\gamma_i$ illustrated in Figure 7 are less than unity across the entire range of acceptable electron gradients. The possible electron $\gamma_e$ range from $\frac{1}{3} < \gamma_e < 1.51$. When the effective $\gamma$ are less than unity, estimates of the size of nonthermal tail strengths that could make this type of local behavior have been made for the ion and electron parameters according to the formula [cf. *Scudder*, 1992a]

$$\kappa_{e,i} = \frac{3 - \gamma_{e,i}}{2 - 2\gamma_{e,i}} = \frac{\beta_{e,i} - 2\beta_i + 8}{2\beta_{e,i}}. \tag{34}$$

These are illustrated in Figure 8. Of note is that all the ion $\kappa_i$ estimates are below 5 and most are of a range similar to those suggested by *Scudder* [1992b] to be required for the formation of the coronal lines with excess Doppler width and for the supply of the ion number flux into the solar wind [*Scudder*, 1994] indicated by the labeled interval "velocity filtration" (Figure 8).

## 5. Two-Fluid Unequal Temperatures at the Critical Point

Since the electron and ion temperatures need not be in equilibrium at the critical point, the results above are further generalized for the circumstance

$$\langle T_* \rangle = \tfrac{1}{2}(T_{e*} + T_{i*}), \tag{35}$$

while the radial variations are assumed to be independent as well, viz.,

$$T_{e,i} = T_{e*,i*}\left(\frac{r}{r_*}\right)^{\beta_{e,i}}. \tag{36}$$

In this circumstance the two-fluid critical point occurs at

$$r_* = \frac{GM_S(M + m)}{2k\langle T_* \rangle[2 - (\beta_e \Delta_e + \beta_i \Delta_i)]}, \tag{37a}$$

where the $k$th species partial pressure is defined to be

$$\Delta_k = \frac{T_{k*}}{T_{e,*} + T_{i,*}}, \tag{37b}$$

and where

$$\Delta_e + \Delta_i \equiv 1. \tag{37c}$$

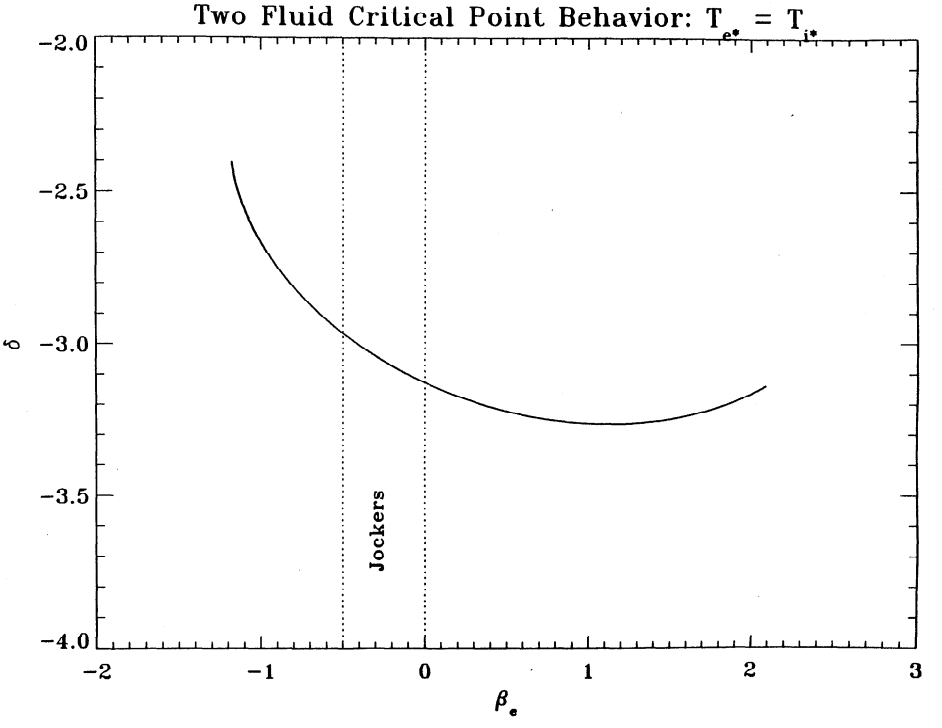


**Figure 6.** Two-fluid common temperature: logarithmic scale length $\delta$ of the density at the critical point for the solution sets of Figure 3.

In the previous section of equal temperature at the critical point, $\Delta_k = \frac{1}{2}$ and (37a) reduces to (27).

The condition on the equality of the two-fluid critical point and the exospheric minimax location generalizes to the expression

$$4 - 2\beta_e\Delta_e - 2\beta_i(1 - \Delta_e) = 2\Delta_e(-\delta - \beta_e). \quad (38a)$$

Using the continuity relationship to eliminate $\delta$ in (38a) implies that

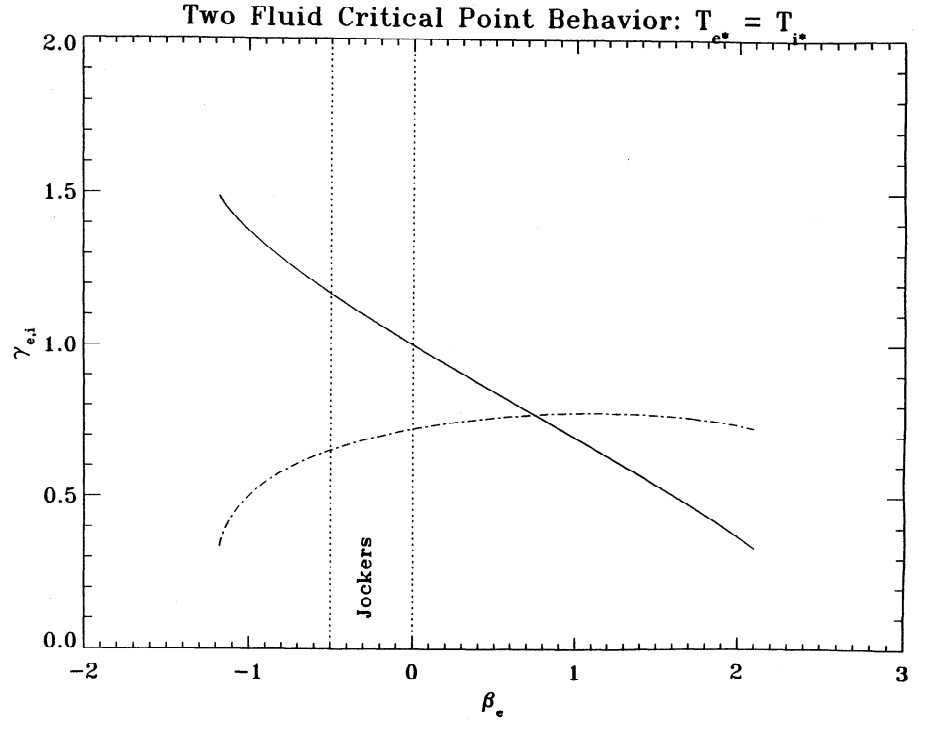


**Figure 7.** Two-fluid common temperature: effective polytrope exponent required at the critical point versus $\beta_e$: $\gamma_i$, dashed; $\gamma_e$, solid.

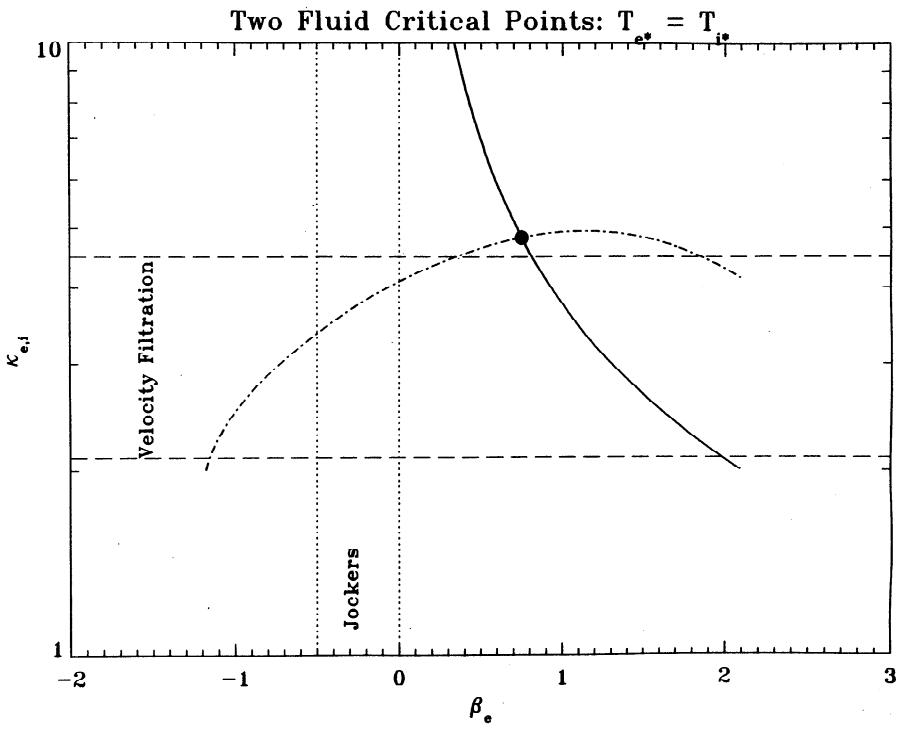


**Figure 8.** Two-fluid common temperature: estimates of $\kappa_{e,i}$ whenever $\gamma_{e,i} > 1$.

$$\left.\frac{dv}{d\chi}\right|_1 = \frac{(2-\beta_i)(\Delta_i)}{\Delta_e} > 0. \tag{38b}$$

This latter condition (as in the restricted two-fluid case) again implies that $\beta_i < 2$ and $\Delta_i > 0$ is required for the accelerating solution. This condition is superseded by the $\gamma_i > \frac{1}{3}$ requirement that implies $\beta_i < 8/5$ is required.

The l'Hospital condition determines the condition on the acceleration at the critical point. The generalization of (29) in dimensionless units becomes

$$2\left(\frac{dv}{d\chi}\right)^2\Big|_1 - \left.\frac{dv}{d\chi}\right|_1 (\beta_e\Delta_e + \beta_i\Delta_i)$$
$$+ [\Delta_e(\beta_e - 2)(\beta_e + 1) + \Delta_i(\beta_i - 2)(\beta_i + 1)] = 0. \tag{39}$$

Substituting (38b) into (39) and using (37c) to eliminate $\Delta_i$ yields the following quadraticform,relatingtheallowable$(\beta_i, \beta_e)$ pairs that satisfy $r_* = r_{\Psi_+}$, parametric in the assumption of $\Delta_e$:

$$\beta_i^2(2 - 3\Delta_e + \Delta_e^2) + \beta_i[-8 + 14\Delta_e + \Delta_e^2(\beta_e - 5) - \Delta_e^3(1 + \beta_e)]$$
$$+ [8 - 16\Delta_e + (6 - 2\beta_e)\Delta_e^2 + (\beta_e + \beta_e^2)\Delta_e^3] = 0. \tag{40}$$

The condition that both roots of (39) are real and of opposite sign reduces to the condition that $(\beta_e, \beta_i)$ are on (40) but inside an ellipse determined by the inequality

$$\frac{(\beta_e - \frac{1}{2})^2}{9/(4\Delta_e)} + \frac{(\beta_i - \frac{1}{2})^2}{9/(4\Delta_i)} < 1, \tag{41}$$

that generalizes (30). We retain (31e)–(31g) as constraints.

We now consider a sequence of models with differing electron partial pressures at the critical point: $\Delta_e = \{0.05, 0.15, 0.25, 0.35, 0.45, 0.55, 0.65, 0.75, 0.85, 0.95\} = 1 - \Delta_i$ to ascertain the implications for the radial temperature exponents at the critical point.

No critical points could be found unless the electron partial pressure fraction $\Delta_e$ at the critical point temperature exceeds a critical level given by the condition

$$\Delta_e > \Delta_* = \equiv 0.242 \tag{42a}$$

(existence of critical points), that translates into the requirement that

$$T_{e*} > 0.319 T_{p*} \tag{42b}$$

(existence of unequal temperature critical points).

Above $\Delta_*$, a range of acceptable electron and ion temperature gradients could be found, as illustrated in Figure 9. Each distinct curve corresponds to a different choice of $\Delta_e$ from the above list. The uppermost curve that is almost horizontal corresponds to $\Delta_e = 0.25$; curves beneath this one correspond to increasing electron fractions of critical point temperature with an increment of 0.1, with the most curvilinear trace corresponding to $\Delta_e = 0.95$. Unlike the two-fluid equal temperature results of Figure 9, there are regimes of $\Delta_e$ where the ion temperature gradient can be negative at the critical point. These regimes where $\beta_i < 0$ correspond to $\Delta_e \simeq 0.7$ and would correspond to a critical point with $T_e > (7/3)T_p$. In the limit of $\Delta_e \to 1$, $T_{p*} \to 0$, so that these are very cold, slow critical point solutions that are not appropriate for the observed solar wind. Under this most general examination of the critical point requirements there is not a major shift in the possible range of electron temperature variations. As illustrated in Figure 9, Parker's original interval $-1 < \beta_e < 2$, includes nearly all possible $(\beta_e, \beta_i)$ gradient pairs.

The range of acceleration possible under this enlarged crit-

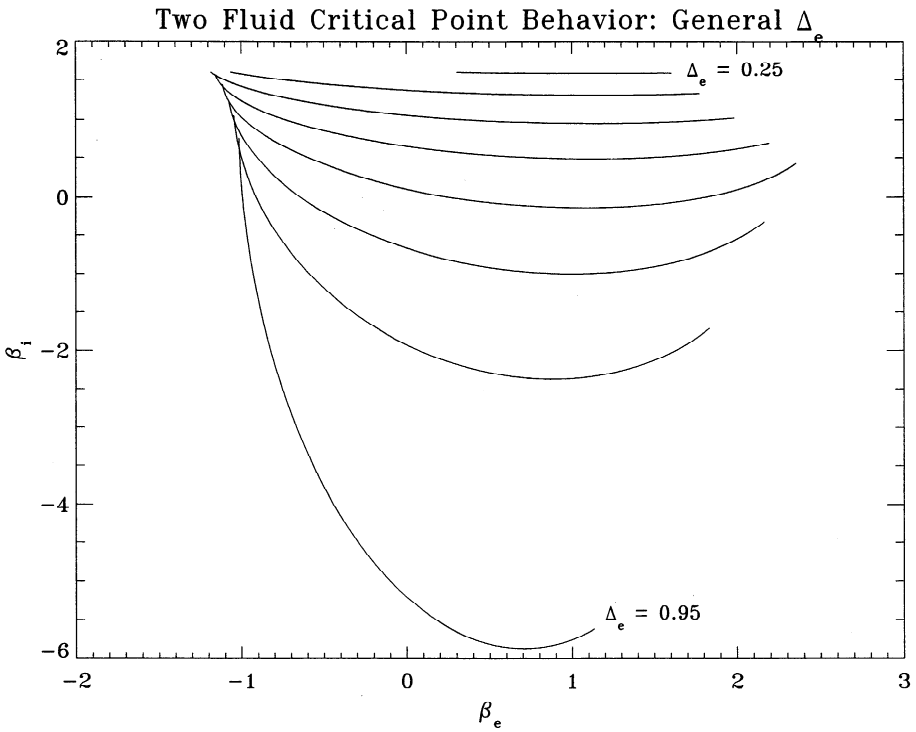


**Figure 9.** Two-fluid general temperatures: ($\beta_e$, $\beta_i$) with critical points. Different curves correspond to different assumed fractions of electron temperature at the critical point.

ical point discussion is illustrated in Figure 10, using the same family of $\Delta_e$ curves that were illustrated in Figure 9. Unlike the ($\beta_e$, $\beta_i$) curves, the acceleration curves are not nested by choice of $\Delta_e$, since this factor enters the determination of the acceleration (cf. (38b)). The smallest $\Delta_e = 0.25$ acceleration trace is shorter in $\beta_e$ extent and relatively high in the family of acceleration curves. As $\Delta_e$ increases, the apexes of the curves first rise and then fall, with the maximum acceleration profile

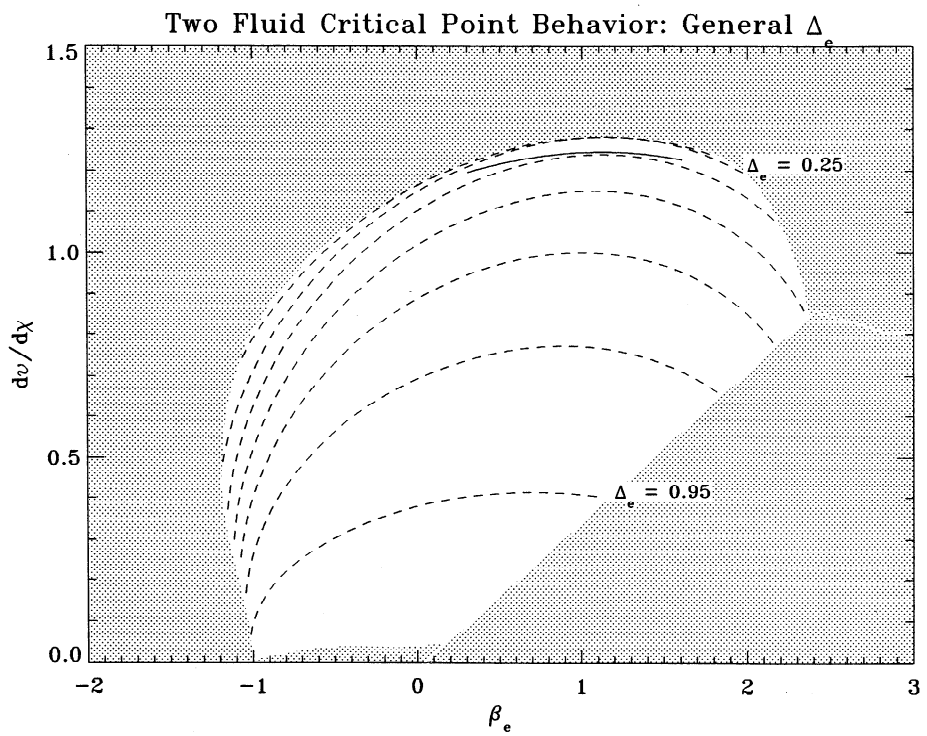


**Figure 10.** Two-fluid general temperatures: fluid acceleration, $(dv/d\chi)|_{\chi=1} = (2 - \beta_i)(\Delta_i/\Delta_e)$, contoured versus $\beta_e$, for a range of $\Delta_e$. Solid trace occurs at minimum illustrated $\Delta_e = 0.25$.

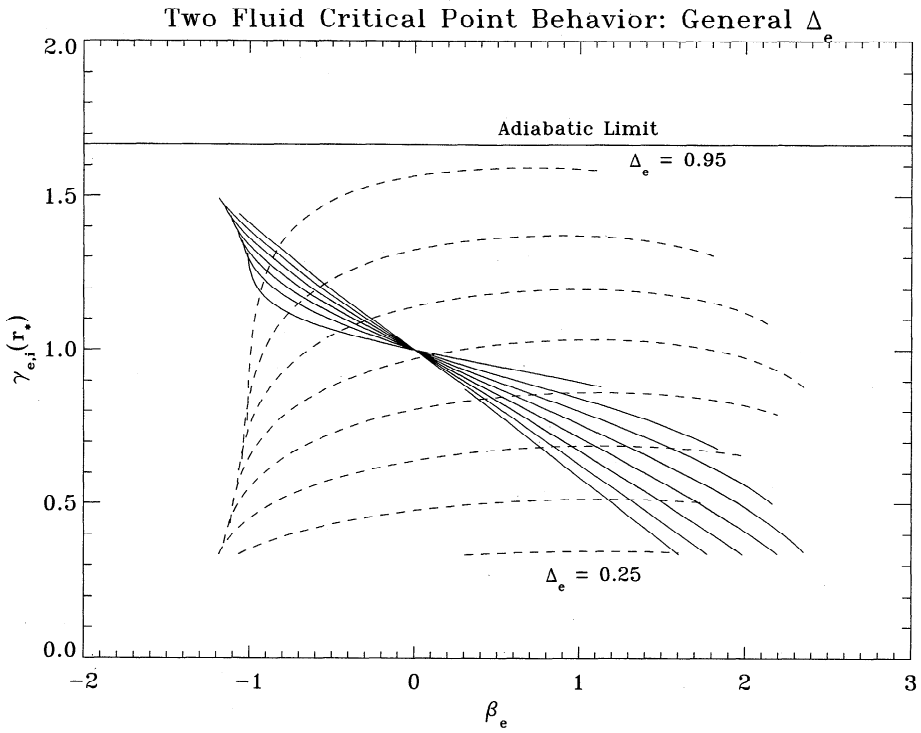


**Figure 11.** Two-fluid general temperatures: effective polytrope exponent required at the critical point versus $\beta_e$, parametric in $\Delta_e$. Traces with common domains of definition correspond to the same $\Delta_e$. The shortest such domain corresponds to $\Delta_e = 0.25$: $\gamma_i$, dashed; $\gamma_e$, solid.

occurring at $\Delta_e = 0.3996 \pm 0.0001$, where the acceleration extrema was found to be

$$\left.\frac{dv}{d\chi}\right|_{\Delta_e=0.3996,\beta_e\simeq 1.2} = 1.2857. \quad (43)$$

Note that this occurs at $\beta_i = 1.14$ and $T_{e*} \simeq 0.66 T_{i*}$. The shaded region of the figure denotes the $(\beta_e, \beta_i)$ regimes where critical points could not be found when surveying the possibilities at a resolution in $\Delta_e = 0.001$.

The effective ion and electron polytrope constants at the critical point are indicated in Figure 11. Dashed and solid curves occur in pairs with a common domain of definition in $\beta_e$. The shortest interval in $\beta_e$ corresponds to $\Delta_e = 0.25$. As $\Delta_e$ increases, the electron polytrope curves become flatter and extend over a wider range of $\beta_e$. After including $\beta_e = 0$, these curves become more horizontal while pivoting about unity. There is a large volume of parameter space where electron and ion $\gamma$ are less than unity.

The critical point locations are also slightly modified in this context. The contours of Figure 12 depict the critical point location in units of the isothermal critical point as a function of $(\Delta_e, \beta_e)$. The critical point locations are moved by order of 1 factors from the isothermal location. Critical points are moved inside the isothermal location by as much as 20% if $T_{e*} > 4T_{p*}$ and $\beta_e < 0$. The abrupt termination of viable critical points at the leftmost extremity is the $\Delta_*$ boundary noted previously.

## 6. Discussion

The requirements derived by Parker for the existence of a critical point in a spherically symmetric coronal atmosphere are recovered starting from the exospheric point of view. The necessary and sufficient conditions in exospheric theory for the radial sonic critical point $r_*$ to exist are that the ion's equivalent potential $\Psi_+$ should be positive at $r_*$ and possess a local maximum there. Supposing that $\Psi_+$ has such a profile at the critical point, together with the requirement that the flow speed be an increasing function at $r_*$, is sufficient to derive all of the conditions Parker demonstrated to accompany the formation of an X-type critical point using the average, or one-fluid, equations. Having established this equivalence, it is clear that the implied constraints of the local variation of the one-fluid temperature derived by Parker are really constraints on the electron temperature behavior near the critical point, which in turn, controls the size and form of the electrical potential. Within this one-fluid model a unique radial temperature gradient for electrons and ions is required with power law exponent $\beta = \frac{3}{4}$. A two-fluid analysis of the critical point formation has been conducted that exploits the complementary views of the critical point afforded by the present association. It is shown that the location of the critical point is determined by the one-fluid temperature and the partial pressure average of electron and ion temperature radial exponents. The value of the fluid acceleration at the critical point is controlled by the ion temperature gradient $\beta_i$ and the fraction of the critical point temperature found in the ions, $\Delta_i$.

The required spatial gradients of speed, density, and electron and ion temperature required to form quasi-neutral X-points in the flow allows determination of the effective polytrope $\gamma$ required in the vicinity of the critical point. Of particular interest is the result that all critical points with common electron and ion temperature required $\gamma_i < 1$, a behavior that the previously suggested mechanism of velocity

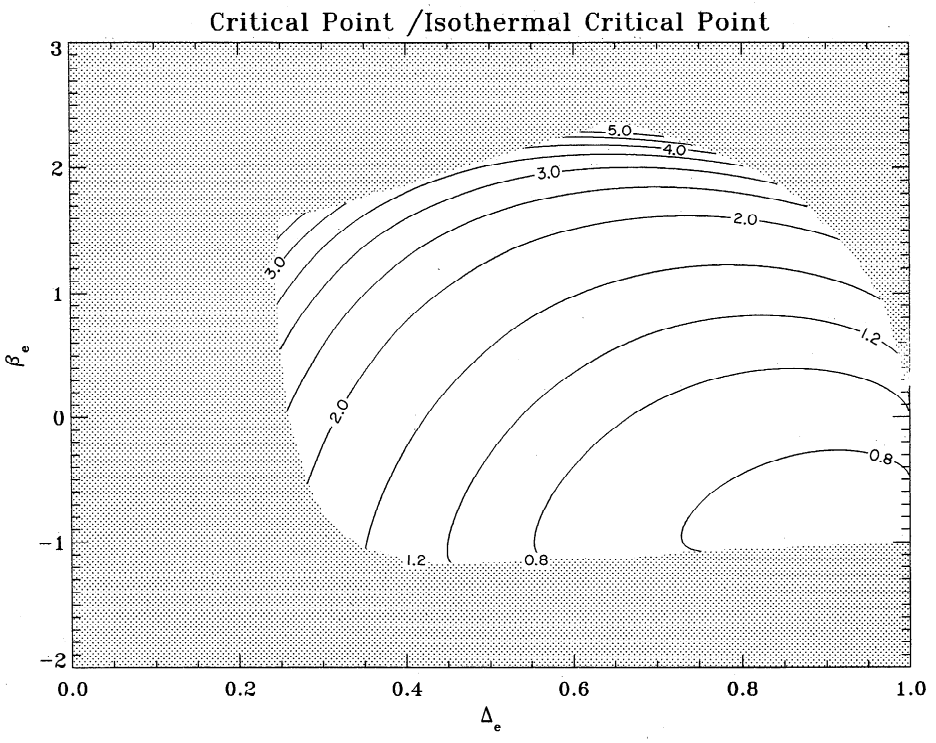


**Figure 12.** Two-fluid general temperatures: contour of critical point locations in units of the isothermal critical point location as function of $\Delta_e$ and $\beta_e$.

filtration can produce [*Scudder*, 1992a, b, 1994]. Radial ion temperature exponents $\beta_i$ at the critical point vary between 0.859 and 1.60. Many, but not all, of these same solutions also correspond to electron $\gamma_e$ less than unity. The electron exponents ranged from $-1.12$ to 2.09. If electron and ion temperatures are very unequal and electrons are hotter, $\gamma_i > 1$ are suggested, although most circumstances require electron and ion $\gamma_\pm < 1$, a regime of plasma behavior that is possible in a retarding potential. Whatever the assumption of the relative size of the required electron and ion temperature at the critical point, the electron temperature exponents are rarely outside the original Parker inequality of $(-1 < \beta < 2)$; when they exceed this limit, they do so only by 10%. The maximum acceleration occurs when the electron temperature at the critical point is approximately two thirds the ion temperature and the electron temperature is still rising at the 1.1 power of the radial distance.

When $\gamma < 1$, estimates have been made of the range of nonthermal distributions required to produce this type of anticorrelated temperature and density behavior. The inferred distributions are shown to be significantly removed from the Gaussian shape with approximately the same nonthermal strength as required from excess Doppler line widths and arguments of energy balance [*Scudder*, 1992b]. For common temperatures at the critical point, all ion nonthermal tail strengths $\kappa$ are less than 5, on a scale where $\infty$ is a Maxwellian. Electron and ion behavior for critical point phenomena down to and including those very near 2 can be realized. In this way, strong ancillary support for the need for nonthermal tails is found in the required steady state behavior of ions and electrons near the critical point.

The mathematical deLaval rocket engine analogy is more appropriately associated with the velocity space barrier to free ion expansion made by the equivalent ion potential near the critical point (cf. Appendix B). Paradoxically, the higher equivalent potential barrier necessary for quasi-neutrality in the presence of expansion performs a velocity space selection that enhances the average speed of that smaller group of particles that surmount the obstacle. Because the number flux is conserved regardless of the form of the potential, the reflection of the lower energy ions at this barrier lowers the number of ions that can carry the conserved number flux. This effect is a consequence of velocity filtration [*Scudder*, 1992a] on the ions. From this microscopic force perspective, the crucial role of "velocity filtration" is demonstrated in the acceleration and heating of the wind and that they are coordinated aspects of the same problem: kinematic access in the coherent forces. In this way, a microphysical discussion from a quasi-neutral plasma description (not possible from the gasdynamic fluid discussion of Parker) can be obtained of the heating, acceleration, and velocity space selection of those particles that compose the solar wind expansion.

## Appendix A: Nature of the Zero Numerator of (2)

For simplicity, consider the isothermal one-fluid case to simplify the treatment. The one-fluid equation with $P = 2nkT$ in the form of the steady state momentum equation is

$$\rho U \frac{dU}{dr} = -2kT \frac{dn}{dr} - \rho \frac{GM_S}{r^2}. \tag{A1}$$

Solving the expression of conservation of mass flux for the density and substituting it into (A1) yield

$$U \frac{dU}{dr} - \frac{4kT}{(M+m)r} + \frac{2kT}{(M+m)} U^{-1} \frac{dU}{dr} - \frac{GM_S}{r^2}. \tag{A2}$$

The first two terms on the right-hand side of (A2) are the expansion of the density gradient of (A1) and represent the pressure gradient force arising from the change in density, which through conservation of mass is transformed into (A2).

The complete right-hand side of (A2) describes the competition between the total fluid pressure gradient and gravity. To achieve the critical point form, the terms involving the bulk speed gradients are regrouped together, which distributes the pressure gradient force between the left- and right-hand sides:

$$\left(U^2 - \frac{2kT}{(M+m)}\right) U^{-1} \frac{dU}{dr} = \frac{4kT}{(M+m)r} - \frac{GM_S}{r^2}. \qquad \text{(A3)}$$

Solving for the acceleration yields (2) of the text. Notice that the location where the numerator of (2) (or the right-hand side of (A3)) vanishes is where the gravitational potential energy equals $4kT$, viz.,

$$\frac{GM_S(M+m)}{r_*} = 4kT, \qquad \text{(A4)}$$

a result not transparently the same as the balance point between gravitational force and electrical force on an ion. This difference of form arises because individual particles do not respond to the collective pressure gradient force (but the electric field it defines), together with magnetic and gravitational forces. The physics of the wind sonic critical point can be delineated more precisely by understanding that it is caused by the change in shape of the equivalent potential for ions at this location.

## Appendix B: The Sonic Critical Point as a Velocity Space deLaval Nozzle

A classical deLaval nozzle shapes the expansion of a gas by an appropriate choice of the confining container. The resulting efficient acceleration of the gas results from the statement of continuity of matter in a channel of varying cross-sectional area $A(s)$:

$$n(s)V(s)A(s) = C.$$

The gas is accelerated at the constriction in the cross-sectional area. The proper choice of the shape of this channel and elimination of back pressure on the flow permit a supersonic expansion to result. *Parker* [1963] has summarized *Clauser*'s [1961] point about the wind expansion resembling a deLaval nozzle. Appeal was made to the deLaval aspect of Bernoulli's equation that is the foundation of the solar wind equations. These two problems have the common mathematics of critical points of the Bernoulli equation. In this paper the velocity filtration of an ionized gas as it undergoes expansion in a gravitational field is contrasted with the configuration space constriction of the deLaval nozzle of a rocket engine. This distinction is not artificial, since in the actual rocket engine, all the matter that starts along the axis of the rocket throat continues to make progress along the axis to the rocket aperture. As the nozzle converges, the particles move faster to conserve the number flux that emerges. At Parker's sonic point in the solar wind there is no configuration space channel that is shaped to make the transition go supersonic. Further, all the particles moving upward below the sonic point do not remain in the wind beyond the supersonic point. (Shaping $\nabla|\mathbf{B}|$ lower in the corona does make a strictly analogous deLaval channeling as recovered by *Pneumann and Kopf* [1971].)

**Acknowledgments.** This work has been partially supported by NSF grant ATM 93-20623. Manuscript comments by the referee and J. Dorelli are also acknowledged.

The Editor thanks M. Schulz and another referee for their assistance in evaluating this paper.

## References

Brandt, J. C., and J. P. Cassinelli, Interplanetary gas 11: An exospheric model of the solar wind, *Icarus*, *5*, 47–63, 1966.

Chamberlain, J. W., Interplanetary gas 2: Expansion of a model solar corona, *Astrophys. J.*, *131*, 47–56, 1960.

Chamberlain, J. W., Interplanetary gas 3: A hydrodynamic model of the corona, *Astrophys. J.*, *133*, 675–687, 1961.

Chamberlain, J. W., On the existence of slow solutions in coronal hydrodynamics, *Astrophys. J.*, *141*, 320–322, 1965.

Clauser, F. H., Questions of general background and methodology relating to aerodynamic phenomena in stellar atmospheres, *Nuovo Cimento*, *22*, *suppl.*, 1, 1961.

Eviatar, A., and M. Schulz, Ion-temperature anisotropies and the structure of the solar wind, *Planet. Space Sci.*, *18*, 321–332, 1970.

Hollweg, J. V., Collisionless solar wind, 1, Constant electron temperature, *J. Geophys. Res.*, *75*, 2403–2418, 1970.

Hollweg, J. V., Collisionless solar wind, 2, Variable electron temperature, *J. Geophys. Res.*, *76*, 7491–7502, 1971.

Jensen, E., Mass losses through evaporation from a completely ionized atmosphere with application to the solar corona, *Astrophys. Norv.*, *8*, 99–126, 1963.

Jockers, K., Solar wind models based on exospheric theory, *Astron. Astrophys.*, *6*, 219–239, 1970.

Krall, N., and A. Trivelpiece, *Principles of Plasma Physics*, McGraw-Hill, New York, 1973.

Lemaire, J., and M. Scherer, Model of the polar ion exosphere, *Planet. Space Sci.*, *18*, 103–120, 1970.

Lemaire, J., and M. Scherer, Kinetic models of the solar wind, *J. Geophys. Res.*, *76*, 7479–7490, 1971.

Pannekoek, A., Ionization in stellar atmospheres, *Bull. Astron. Inst. Neth.*, *1*, 107–118, 1922.

Parker, E. N., Dynamics of the interplanetary gas and magnetic fields, *Astrophys. J.*, *128*, 664–676, 1958.

Parker, E. N., *Interplanetary Dynamical Properties*, Wiley-Interscience, New York, 1963.

Parker, E. N., Dynamical properties of stellar coronas and stellar winds, I, Integration of the momentum equation, *Astrophys. J.*, *139*, 72–92, 1964a.

Parker, E. N., Dynamical properties of stellar coronas and stellar winds, 2, Integration of the heat flow equation, *Astrophys. J.*, *139*, 93–122, 1964b.

Pneumann, G., and R. Kopp, Gas-magnetic field interactions in the solar corona, *Solar Phys.*, *18*, 258–270, 1971.

Rosseland, S., Electrical state of a star, *Mon. Not. R. Astron. Soc.*, *84*, 720–728, 1924.

Schultz, M., and A. Eviatar, Electron temperature asymmetry and the structure of the solar wind, *Cosmic Electrodyn.*, *2*, 402–422, 1972.

Scudder, J. D., On the cause of temperature change in inhomogeneous low density astrophysical plasmas, *Astrophys. J.*, *398*, 299–318, 1992a.

Scudder, J. D., Why all stars should possess circumstellar temperature inversions, *Astrophys. J.*, *398*, 319–349, 1992b.

Scudder, J. D., Ion and electron suprathermal tail strengths in the transition region: Support for the velocity filtration model of the corona, *Astrophys. J.*, *427*, 446–452, 1994.

Scudder, J. D., Dreicer order ambipolar electric fields at Parker's steady state solar wind sonic critical point, *J. Geophys. Res.*, in press, 1996.

Simmons, G. F., *Differential Equations With Applications and Historical Notes*, p. 306, McGraw-Hill, New York, 1972.

Sturrock, P., and R. E. Hartle, Two fluid model of the solar wind, *Phys. Rev. Lett.*, *16*, 628–631, 1966.

J. D. Scudder, Department of Physics and Astronomy, University of Iowa, 203 Van Allen Hall, Iowa City, IA 52252-1479. (e-mail: jds@space-theory.physics.uiowa.edu)

(Received May 18, 1995; revised October 19, 1995;
accepted January 15, 1996.)